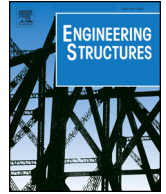




ELSEVIER

Contents lists available at ScienceDirect

Engineering Structures

journal homepage: www.elsevier.com/locate/engstruct

Seismic performance assessment of low-rise precast wall panel structure with bolt connections

Wei Guo^{a,b,c}, Zhipeng Zhai^{a,b,c}, Yao Cui^{d,*}, Zhiwu Yu^{a,b,c}, Xiaoli Wu^{a,b,c}

^a School of Civil Engineering, Central South University, Changsha 410075, China

^b National Engineering Laboratory for High Speed Railway Construction, Changsha 410075, China

^c Engineering Technology Research Center for Prefabricated Construction Industrialization of Hunan Province, Changsha 410075, China

^d State Key Laboratory of Coastal and Offshore Engineering, Dalian University of Technology, Dalian 116024, China

ARTICLE INFO

Keywords:

Precast structure
Bolt connection
Shaking table test
Seismic performance
Fragility

ABSTRACT

This paper proposes a novel low-rise precast wall panel structure with bolt connections, which has advantages of convenient and rapid assembly. To investigate seismic performance of the structure system, a shaking table test of a 1/2 scaled three-story model is conducted, by which the structural dynamic responses, damage pattern, and seismic fragility are analyzed. The results show that the proposed novel precast structure system presents high stiffness, high load capacity and high collapse margin ratio. In this novel structure system, the bolt connections are critical for the structural dynamic characteristics and responses. Damage pattern of the structure follows the sequence of bolt loosening, adjoining wall panels sliding and dislocating, structural components cracking. The seismic damage of test structure is slight, and most structural components still remain elastic in maximum considered earthquakes. Based on the test results, performance design objectives for service level earthquake, design based earthquake and maximum considered earthquake are given, and four limit states are defined. The fragility curves of the structure are developed, as well as the fragility of nonstructural components.

1. Introduction

Precast building refers to the building whose structural members are precast in factory or construction site, and is assembled by reliable connections. Some references have revealed that precast building can reduce 2/3 waste generation rate, 10% carbon emission, and massive construction cost caused by labor and time cycle [1–3]. Due to these advantages, precast building is widespread in many countries and regions worldwide, such as Europe, the United States, Japan, China, and Malaysia [4,5]. In the last decades, researches on precast building's seismic performance have been systematically carried out [6–9], some of which show that structure adopting precast reinforced concrete shear walls as the main lateral force resistance presents a good seismic performance [8,9]. At present, a variety of precast wall panel structure system have been reported, such as unbonded post-tensioned precast concrete shear walls structure [10–12], steel-concrete composite shear wall structure [13], shear wall structure with metal bellows grouting [14], and new types of sandwich and light-weight wall structure [8,15–19]. The precast concrete shear wall structure has a great potential in the development of residential building industrialization.

Low-rise residential building is generally the main type in the rural

area worldwide. Different structural systems have been proposed and corresponding seismic performances are also studied. Theoretical research can give a approximate estimate of seismic performance and risk of structure [20], and numerical simulation [21–23] provides meaningful results for some specific problems which are hard to be implemented in the lab. However, the most valuable data and effective approach to investigate the mechanical performance of structures is the model test and in-situ test [24–29]. Brunesi [4] proposed a new type of lightly reinforced concrete precast shear wall structure for low-rise residential building, which is connected by threaded anchors and bolts. The seismic performance and damage pattern of the shear wall were studied by the pseudo static test, and it showed that there's large residual deformation in the connection joints. Xu [6] has conducted quasi-static test to verify the validity of sleeves connection to be used in precast shear wall. The maximum inter-story drift angle of the precast specimen approached 1/56. And the results showed that the precast specimen behaved similarly to the cast-in-situ specimen with respect to failure mode, inter-story drift angle, ultimate force, ductility, stiffness degradation and energy dissipation capacity. Gavridou [30] carried out a shaking table test of a full-scale post-tensioned concrete wall building, and under strong earthquake excitation the structural damage was

* Corresponding author.

E-mail address: cuiyao@dlut.edu.cn (Y. Cui).

<https://doi.org/10.1016/j.engstruct.2018.12.060>

Received 4 July 2018; Received in revised form 30 November 2018; Accepted 17 December 2018

0141-0296/ © 2018 Published by Elsevier Ltd.

repairable and no pre-stress loss was found despite the interface grout crushed partially. Lim [31] presented a type of precast concrete T-wall structural system with C-shaped steel plate connected, and the seismic performance and connection's reliability were verified by quasi-static test.

In the low-rise precast shear wall structure systems mentioned above, the connection joints are generally the core components, and the dry connection such as steel plate and bolt is preferred [32]. An O-connector [33] made by mild steel, which has good capacity of energy dissipation and ductility, was proposed and studied by the connection test. Bournas [34,35] utilized two thick steel plates and bolts to connect the longitudinal rebar of the joints, and the tensile test for this connection showed the good ductility and the failure mode of the longitudinal rebar. Bora [36] invented a joint connection composed of steel plates, brass plates and bolts. Similarly, Lago [7] used steel plates, brass plates and bolts to connect the embedded angle steel. Both of them are proven to have the good hysteresis performance and energy dissipation capacity by the laboratory test.

The dry connection has been proven to be effective in the low-rise precast wall panel structure system. In this paper, a new type of dry connection utilizing high strength bolt and steel plate is proposed, and accordingly a low-rise precast wall panel structure with bolt connections (LPWSBC) is introduced. In order to investigate the seismic performance of LPWSBC, a 1/2 scaled three-story model is constructed for shaking table test. The behavior of specimen under service level earthquake (SLE), design based earthquake (DBE), and maximum considered earthquake (MCE) in the high seismic intensity region are considered in the test. And the bidirectional excitations of ground motions are also taken into account. By the test, the dynamic responses and the damage pattern of LPWSBC are given. Moreover, the reliability of the bolt connection, seismic performance and fragility of LPWSBC are analyzed.

2. Description of the LPWSBC

Fig. 1 shows the basic configuration of the low-rise precast wall panel structure with bolt connections (LPWSBC), which has an advantage in the construction speed. The concrete walls are connected by the dry connections and work as a box structure to transfer the gravity

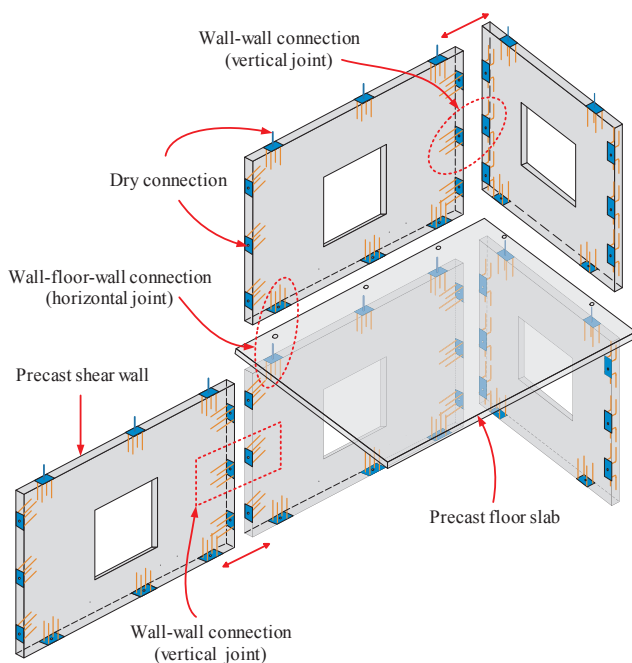


Fig. 1. LPWSBC structure system.

load and lateral load. Generally, three types of concrete walls could be adopted in such system, including normal concrete solid wall, light aggregate concrete solid wall and foam sandwich wall. In this research, the light aggregate concrete solid wall is selected due to the advantage of lightness.

The dry connection in LPWSBC consists of an anchored steel plate (Q345 steel with the nominal yield strength of 345 MPa) and high strength bolt (Grade 10.9 high-strength bolt with the nominal yield strength of 900 MPa). It is classified into the horizontal joint and vertical joint, as shown in Fig. 2. The horizontal joint is the connection between the precast wall and foundation (Fig. 2(a)), and the connection between top and bottom precast walls (Fig. 2(b)), in which the high-strength bolt will pass through the floor slab to connect the two precast walls. The vertical joint is the connection along the height of two precast walls and the connection between precast floor slabs. As shown in Fig. 2(c) and (d), depends on the positions of the walls, it includes three types of connection: “F” Type, “L” Type, and “T” Type. The “F” Type vertical joint is also used to connect the precast floor slabs.

In this structural system, the gravity load is transferred from slabs to shear walls, and the lateral load, such as seismic load, is resisted by shear walls and horizontal joints. The seismic load resisted by each floor slab under different shaking intensity is calculated according to Chinese code for seismic design of buildings [37], and it is distributed to each wall. According to Chinese code for design of steel structures [38] (hereafter steel code), the number of high strength bolts for horizontal joint of each wall then can be designed by the following formulas:

$$N_v^b = 0.9n_f\mu P \quad (1)$$

$$n = \frac{V}{N_v^b} \quad (2)$$

where n is the number of the connection; N_b is the design value of shear capacity of a single high strength bolt; V is the lateral force of the wall; n_f is the number of friction surface, which equals to 1 here; μ is the friction coefficient, which is 0.4 according to the steel code [38]; P is the pretension force of high strength bolt, which is given in the steel code [38] based on the diameter of high strength bolt. Moreover, the number of the horizontal joint of each wall should follow the constructional requirements that the connections should be arranged symmetrically along the width of wall and the stability during the wall panel assembly should be ensured. Meanwhile, the number of vertical joint is determined by the requirement of construction, it's suggested to be 3 or 4 in each end of the wall and is arranged evenly along the wall height. Finally, each high strength bolt for the horizontal joint should be checked by the formulas as:

$$N_t \leq N_t^b, N_t^b = 0.8P \quad (3)$$

$$\frac{N_v}{N_v^b} + \frac{N_t}{N_t^b} \leq 1 \quad (4)$$

where N_t and N_v are the shear and tension force of connection subjected, N_b is the design value of tension capacity of the high strength bolt.

3. Experimental plan

3.1. Test specimen

The prototype of the test specimen is a 3-story residential building which is designed according to the Chinese design codes [37–39] and built in Changsha, China. The configurations of the prototype structure are shown in Figs. 3 and 4. The story height is 2.7 m and the span in X and Y-direction is 7.5 m and 5.1 m, respectively.

Each story of the prototype structure is composed by six pieces of precast walls, as shown in Fig. 3. The thickness of the precast wall is 150 mm. There are four short precast walls (5.1 m in width), named as

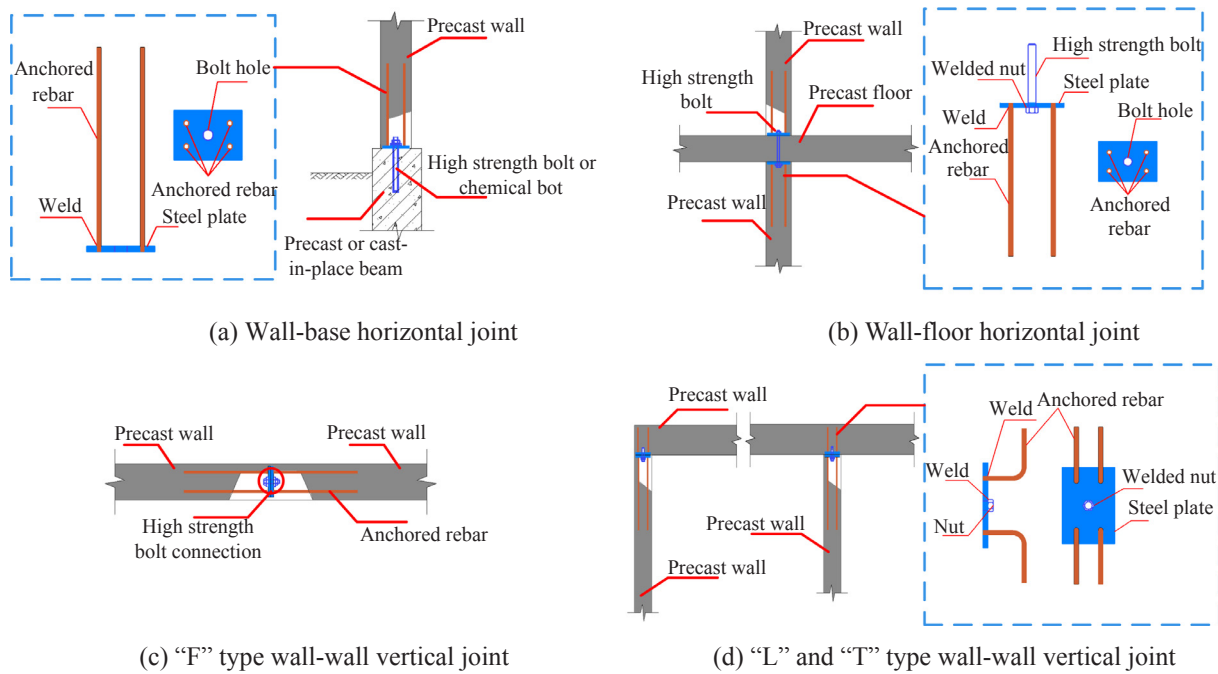


Fig. 2. The schematic plot of main connection joints.

SW1-*i* to SW4-*i* (*i* represents the *i*-th story), in X-direction. The other two longer precast walls (7.5 m in width) are arranged in Y-direction and named as SW5-*i* to SW6-*i*. A stairwell opening exists in the structure, which is also shown in Fig. 3. The light aggregate concrete LC25 with 25 MPa nominal compressive strength and function of heat preservation is used for the precast walls. HRB400 with 400 MPa nominal yield strength is used for the reinforcement.

The precast floor thickness is 150 mm. The arrangement of dry connections is shown in Fig. 4, too. There are four horizontal joints in X-direction and three in Y-direction for each precast wall in every story. There are three vertical joints for each side of precast wall in each story. Therefore, there are 72 horizontal joints and 72 vertical joints in total. In this prototype structure, the anchored steel plate is a 130 mm × 180 mm Q345 steel plate. The thickness of the steel plate is 14 mm and 12 mm for horizontal and vertical joints, respectively. The diameter of 12 mm HRB400 steel bars (nominal yield stress is 400 MPa) are adopted to anchor the steel plate. The diameter of 24 mm Grade 10.9 high strength bolts are used for all the dry connections.

The Shaking table test is conducted in Central South University, China. The shaking table array system is composed of four shake tables, and each table is 4 m length and 4 m width, and can produce 6 degrees of freedom (DOFs). The maximum payload of each table is 30 ton, and corresponding maximum acceleration is 0.8 g and 1.6 g for horizontal and vertical directions, respectively. These tables can be used independently, and can also make up an array system with various adjustable spacing. Considering the capacity of the shaking table, a 1/2 scaled specimen is adopted. In this test, the materials of specimen are the same as the design of the prototype structure. The main parameter's similarity scaling factors of the specimen are shown in Table 1. To ensure the force and displacement similarity, the reinforcement of the structural members and the diameter of high strength bolt are re-designed in accordance with the original design of the prototype structure. The main reinforcement design of the prototype structure and specimen are summarized in Table 2. Fig. 5 shows the detailing reinforcement of the precast wall SW1-1. Most of the detailing reinforcement is laid around the edges of shear walls and the openings. In

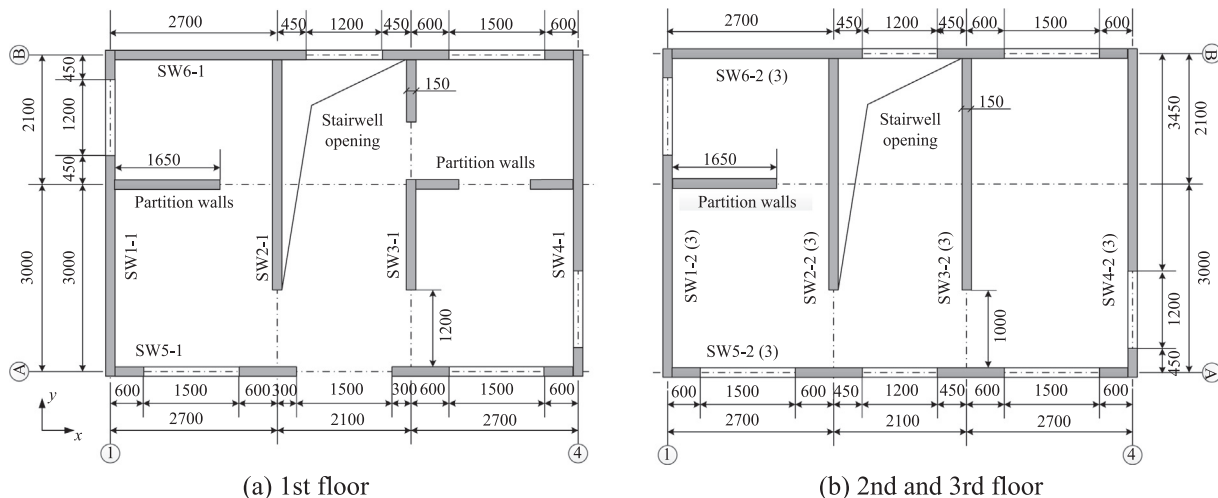


Fig. 3. Floor plan of prototype structure (unit: mm).

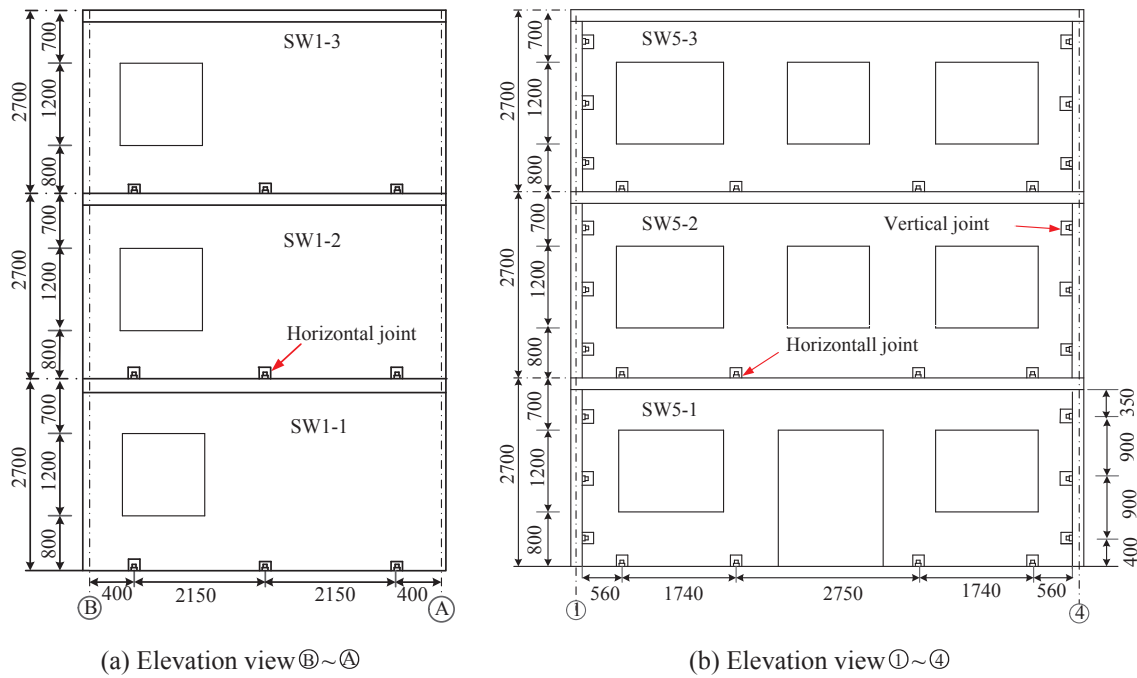


Fig. 4. Elevation view of prototype structure (unit: mm).

the specimen, the size of the steel plate is 75 mm × 110 mm for the dry connection system. For the horizontal and vertical joints, the steel plate thickness and the anchored steel bar diameter are both 8 mm and 6 mm, respectively. High-strength bolts with the diameter of 12 mm are adopted. The partition walls of the prototype structure are treated as the dead load by introducing mass on the corresponding position of the specimen. The measured density and 28-day strength of the light aggregate concrete LC25 are 1960 kg/m³ and 27.6 MPa, respectively. The measured yield strength and ultimate strength for the reinforcement HRB400 steel bar is 400 MPa and 570 MPa, respectively.

To connect the specimen to the shaking table, a rigid reinforced concrete foundation with dimensions of 3.9 m × 2.7 m × 0.35 m is fabricated. The superstructure and the rigid foundation are connected by chemical bolts. Total mass of the specimen is around 21.64 ton, including 13.39 ton for the superstructure, 5.29 ton for the rigid foundation, and 2.96 ton for the dead and live load which are simulated by adding mass blocks. The site operation sequence of the test specimen is as follows: (a) set the rigid foundation in place and fix the foundation on the shaking table, (b) place the precast wall on the foundation beam and set up the brace, then install the bolt to fix horizontal joints, (c) erect other walls of the first floor by the same way as well as the slab, (d) erect the wall panels of the other floors. Fig. 6 shows the construction process of the specimen, and the specimen construction was completed within one day in the laboratory.

Table 1
Similarity scaling factors of the test model.

Parameter	Relation	Scaling factors	Parameter	Relation	Scaling factors
Length <i>l</i>	S_l	0.5	Uniform load <i>q</i>	$S_q = S_\sigma S_l$	0.5
Stress σ	$S_\sigma = S_E$	1.0	Area load <i>p</i>	$S_p = S_\sigma$	1.0
Elastic modulus <i>E</i>	S_E	1.0	Moment <i>M</i>	$S_M = S_\sigma S_l^3$	0.125
Strain ϵ	S_ϵ	1.0	Period <i>T</i>	$S_T = (S_l/S_\sigma)^{0.5}$	0.5
Density ρ	S_ρ	1.0	Frequency <i>f</i>	$S_f = (S_\sigma/S_l)^{0.5}$	2
Mass <i>m</i>	$S_m = S_\rho S_l^3$	0.125	Acceleration <i>a</i>	$S_a = S_E/(S_\rho S_l)$	2
Force <i>F</i>	$S_F = S_\sigma S_l^2$	0.25	Gravitational acceleration <i>g</i>	S_g	1.0

Table 2

The main reinforcement of components in test model and prototype structure.

Components	Prototype structure	Test model	Reinforcement location
Shear walls	D6@250	D4@220	Vertical double layout
		D4@110	Horizontal double layout
Floor slabs	D8@200	D4@100	Double two-way layout
Coupling beams	2D14	2D6	Compression longitudinal reinforcement
		2D16	Tension longitudinal reinforcement
		2D8	Hooping

Note: D represents diameter of HRB400 steel bars; @ represents spacing of steel bars.

3.2. Measurement

The test setup was equipped with accelerometers, laser displacement sensors, and strain gages for measurement with as sampling frequency of 1000 Hz. Fig. 7 shows the locations of the accelerometers and displacement sensors. A total of 16 accelerometers were placed. Four accelerometers, oriented in the X and Y-direction, were installed at the edge of specimen for each floor level as shown in Fig. 7. The accelerometers were used to compute the inertial force applied to the frames. A total of 20 laser displacement transducers were placed. 16 transducers were arranged similar to the arrangement of the accelerometers. The other four transducers, oriented in the Y-direction, were installed at

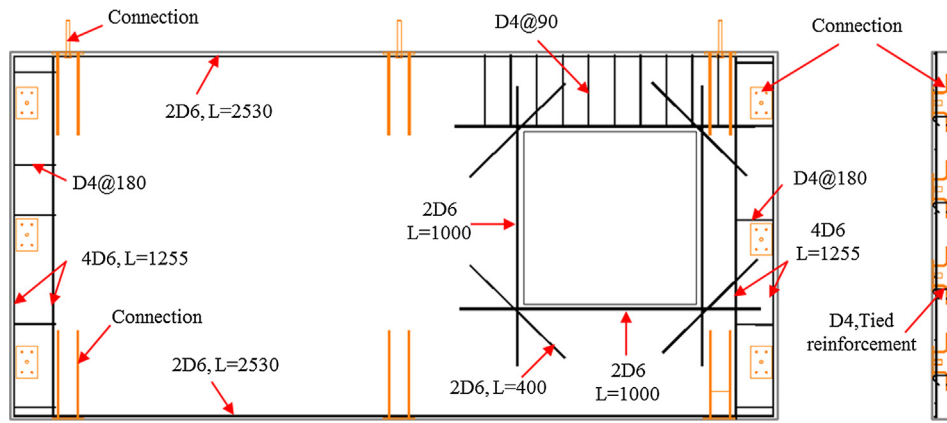


Fig. 5. The detailing reinforcement of shear wall SW1-1 of the test model (unit: mm).

the top and bottom of the precast wall SW1-1 and SW4-1 to measure the relative displacement between the wall and floor slab. Amount of strain gages were attached on the reinforcement of the precast walls and the anchor steel bars to investigate the inelastic behavior of the precast walls and dry connections in the test.

3.3. Loading history

Five ground motions, including Kobe, Taft, Manjil Iran, Whittier Narrows, and an artificial seismic record, are selected according to the natural period of prototype structure. The comparison for response spectrum of the selected ground motions and the design spectrum under

seismic intensity level of SLE is shown in Fig. 8. In the figure, T_1 and T_2 are the fundamental and second period of prototype structure, respectively. Before the ground motions are input, duration and amplitude of the motions would be scaled according to the similarity scaling factors.

The PGA of the input ground motion is increased from 0.10 g, 0.14 g, 0.30 g, 0.40 g, 0.60 g, 0.80 g. For the test structure, the input PGA of 0.14 g, 0.40 g, and 0.80 g represents the seismic intensity level of SLE, DBE and MCE, respectively. For each shaking level, the specimen was first loaded in Y and X-direction, separately. Then, it was loaded in bi-direction and the input PGA ratio of Y to X-direction is 1:0.85. To identify the dynamic characteristics and overall damage state of the structure system, white noise with small magnitude is

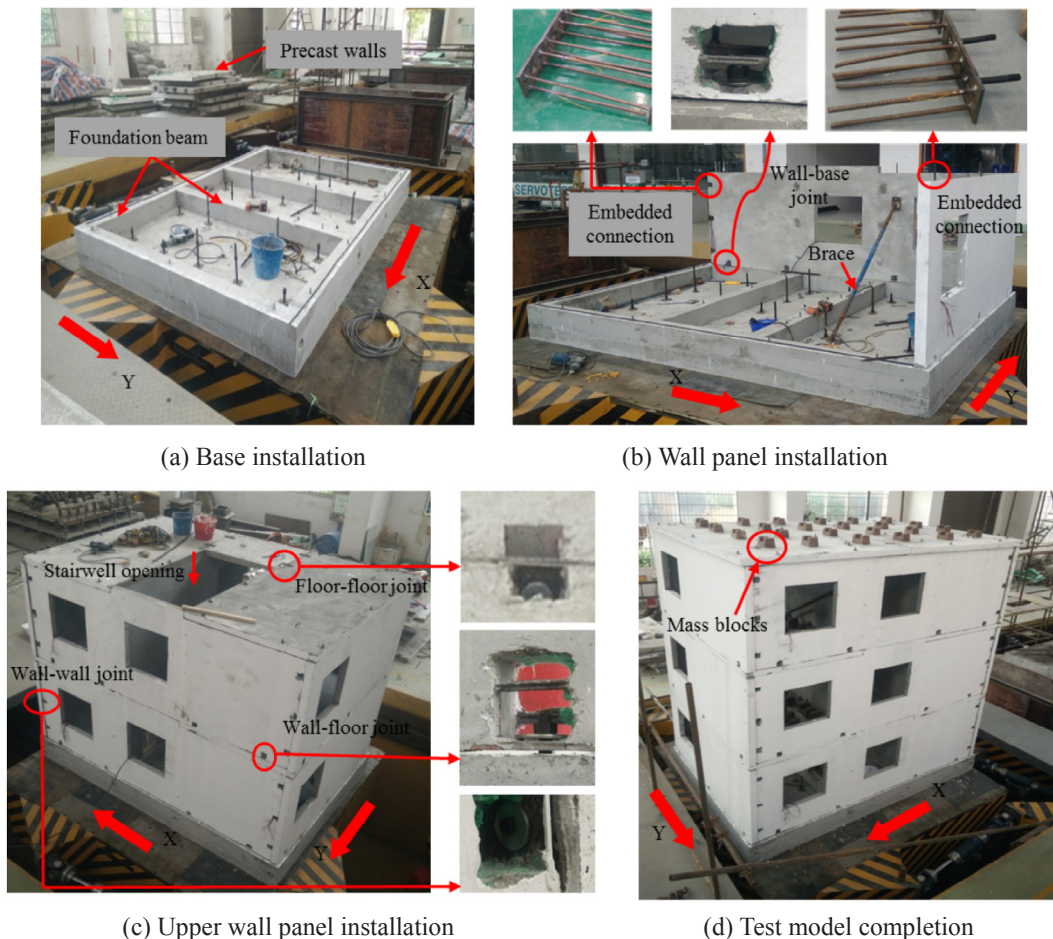


Fig. 6. Process of assembling the test model.

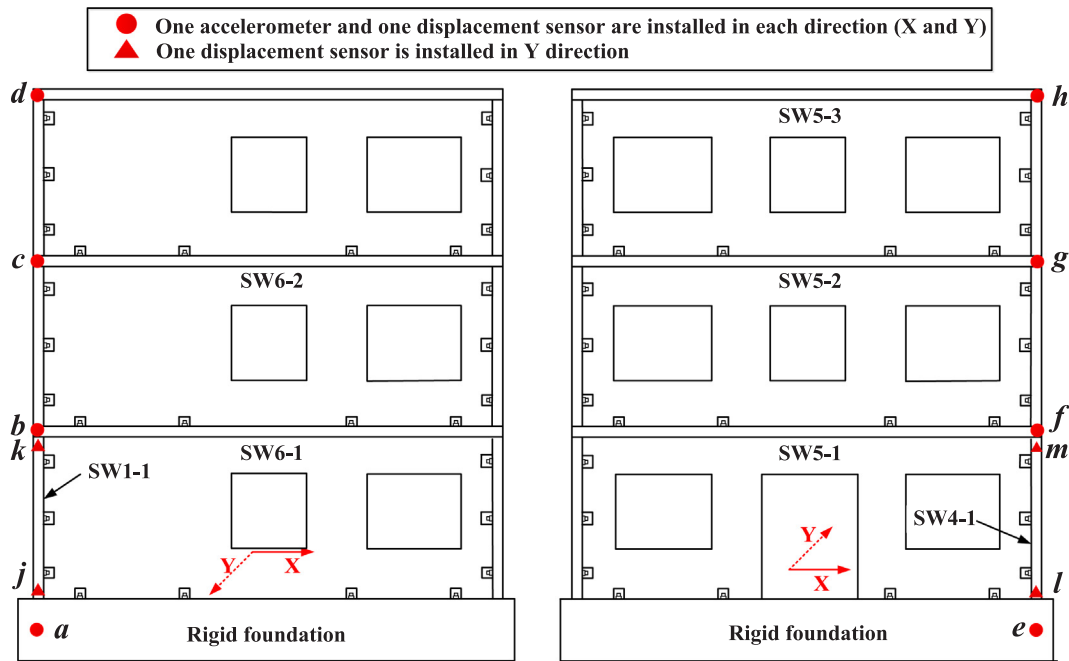
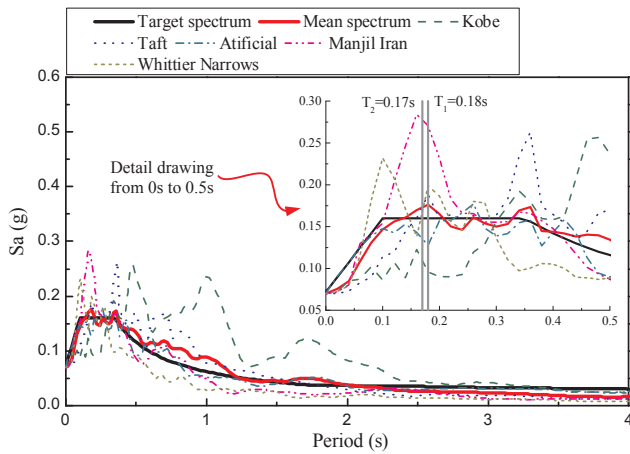
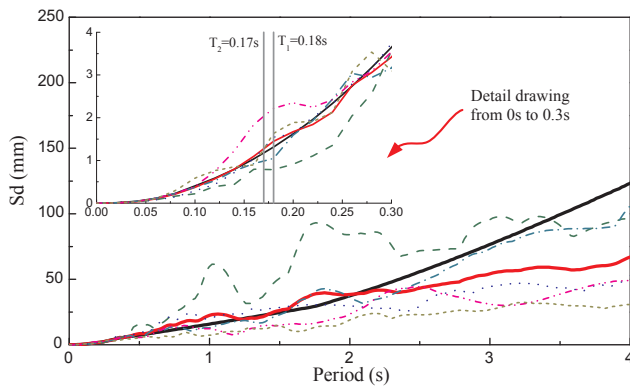


Fig. 7. The layout of accelerometers and displacement sensors.



(a) Acceleration response spectrum



(b) Displacement response spectrum

Fig. 8. Response spectrum of seismic excitations scaled to SLE.

loaded after each seismic level in bi-direction. During the test, 90 seismic loading cases are performed for the 1/2 scaled specimen in total, which are shown in Table 3.

4. Test results and discussions

4.1. Damage observations

The test results showed that the LPWSBC structure had good seismic performance, even under extreme earthquakes. Although some minor cracks were observed around the opening of the precast wall and some local concrete crush were observed at the connection between precast wall and foundation and precast floor slab due to the story sliding, the test specimen stayed almost elastic throughout the whole test.

Damage of the precast wall and floor slab observed in the loading process of shaking table is described as follows. While the loading case 3 with 0.10 g PGA is completed, initial crack of wall SW1-1 is first observed as shown in Fig. 9(a), such crack is initial introduced during the transportation and is not developed in the following loading cases. Under SLE level's excitation with 0.14 g PGA, it is observed that the bolt connection of the wall-to-wall horizontal joint loosen, as shown in Fig. 9(b). And slight sliding between 1st and 2nd story was observed. As the PGA increased to 0.30 g, slight concrete spalled at the interface between precast wall and floor slab (Fig. 9(c)) due to the sliding between each story. Under DBE level's excitation with 0.4 g PGA, structural vibration increased significantly, the sliding between each story increased as shown in Fig. 9(d) and a little parts of rubber pad was squeezed out. The cracks on the exterior walls occurred and propagated (Fig. 9(e)) as the PGA increased to 0.60 g. The concrete spalled of the floor slab was observed, as shown in Fig. 9(f). In addition, the concrete spalled was observed on the interior walls around the horizontal joint, as shown in Fig. 9(g). In the MCE level input with 0.80 g PGA, the cracks were continuing to propagate and new cracks occurred, such as shear cracks on wall SW1-2 and tensile crack on 1st story floor slab, which are shown in Fig. 9(h) and (i). The damage at the interior walls increases, such as concrete spalled and shear cracks propagation on wall SW5-1, as shown in Fig. 9(j).

The damage of connection joints was carefully inspected after the test. No yield or failure of steel plates and anchored steel bars were observed. Slight residual deformation of few anchored bolts of horizontal joint between 1st and 2nd story was observed, as shown in Fig. 9(k). It indicates that the dry connection system showed good seismic performance under extreme earthquakes. Fig. 9(l) shows that

Table 3
Seismic loading cases.

Cases	Earthquake	Direction	PGA (g)	Cases	Earthquake	Direction	PGA (g)
WN	White noise	X,Y	0.07	13	Whittier Narrows	Y	0.1
1	Kobe	Y	0.1	14		X	
2		X		15		X,Y	
3		X,Y		WN	White noise	X,Y	0.07
4	Taft	Y	0.1	16–30	Same sequence as cases 1–15		0.14
5		X		WN	White noise	X,Y	0.07
6		X,Y		31–45	Same sequence as cases 1–15		0.3
7	Artificial	Y	0.1	WN	White noise	X,Y	0.07
8		X		46–60	Same sequence as cases 1–15		0.4
9		X,Y		WN	White noise	X,Y	0.07
10	Manjil Iran	Y	0.1	61–75	Same sequence as cases 1–15		0.6
11		X		WN	White noise	X,Y	0.07
12		X,Y		76–90	Same sequence as cases 1–15		0.8
				WN	White noise	X,Y	0.07

the rubber seal on the first floor slab was squeezed out after the test.

The crack and damage distribution of the structure are also given in Fig. 10. The cracks are few, and the cracks mainly located near the opening, and the width of cracks is relatively small. The obvious structural damages are the crushing and spalling of local concrete caused by compression and slide friction which is significant at the first and second floor. In summary, the whole structural damage is slight, and most of the lateral resistance components remain elastic, so it is speculated that the test structure behaves well under extreme seismic excitation. The main reasons for elastic response of most components are as follows: (a) the bolt loosening isn't considered in the structure design, the wall sliding and friction dissipate a part of earthquake energy as a result of bolt loosening, that's favorable for mitigating the damage of wall and connection components; (b) to meet the requirement of construction and wall assembly, the total number of high strength bolts used for wall-floor joints (horizontal joints) in practice, which is 72, is significantly larger than the value designed from Eq. (2), which is 42.

4.2. Dynamic characteristics

The dynamic characteristics of the test specimen were obtained from the white noise tests. The first two natural frequencies of the test model are recognized and shown in Tables 4 and 5. The first two natural frequencies corresponding to X and Y-direction are 11.154 Hz and 11.688 Hz, respectively. It indicates that the stiffness in X and Y-direction are nearly the same.

In Table 4, it's seen that the frequency of the specimen gradually reduces after the SLE and DBE level's excitations. In the test, in order to prevent the bolt loosening induced failure, the bolts of joint connections are retightened before MCE test. From Table 5, it shows that the natural frequency increases obviously after retightening the bolts, even much larger than that the initial state. The first two frequencies increase from 11.154 Hz and 11.688 Hz to 15.366 Hz and 16.632 Hz, respectively. It confirms that the dry connections are the primary component and have significant influence on the stiffness of the specimen.

The natural frequencies decrease gradually after each test case, and the degradation of frequency indicates the structural damage in a system level. From Tables 4 and 5, the degradation of first natural frequency after SLE, DBE and MCE test case is 1.3%, 10.4% and 19.6%, respectively. And for the second natural frequency that is 4.8%, 11.1% and 18.3%. The degradation of frequency is caused by the bolt loosening and damage of the structural components. As noted in Tables 4 and 5, the first natural frequency after MCE test case is even larger than the initial state. It is indicated that the damage of the structural components is minor, therefore, the degradation of frequency is mainly contributed by the bolt loosen of the dry connections.

4.3. Acceleration responses

The specimen response under SLE, DBE, and MCE level excitation are adopted for the discussion. The Envelope values of each floor's acceleration in the X and Y-direction are plotted in Fig. 11. The responses under one direction and bi-direction loading are shown in Fig. 11(a) and (b), respectively. It is noted that the acceleration response in X-direction is generally larger than Y-direction. And the difference of the acceleration response is minor between one direction and bi-direction loading.

As shown in Fig. 11, the 3rd floor shows the larger acceleration under SLE level input, with the acceleration amplification factor of 2.0–3.5 and 1.7–4.0 for X and Y-direction, respectively. As the input increase to the DBE level (PGA = 0.4 g), the maximum acceleration occurred on the 2nd and 3rd floor in X-direction and Y-direction, respectively. The acceleration amplification factor increased to 2.6–6 in X-direction, while reduced to 1.3–2.2 in Y-direction. Such reduction of acceleration amplification factor is caused by the sliding of the floor.

Under the MCE level input, the maximum acceleration occurs in the 2nd floor and 1st floor in X-direction and Y-direction, respectively. The acceleration amplitude factor is 3.0–6.0 and 2.19–3.0 in each direction. The location of the maximum acceleration is changed due to the sliding of the floor.

Different from the conventional cast-in-site RC shear wall systems, the global stiffness of LPWSBC system is quite high. The acceleration is thereby relatively large. It may be critical to the acceleration-dependent nonstructural components, such as freestanding cabinet.

There is no difference of acceleration response between one direction loading and bi-direction loading. It is further illustrated the primary resistance mechanism of the LPWSBC is the sliding instead of the shear resistance of the precast wall, since the stiffness of sliding is direction independent.

4.4. Displacement responses

The Envelope values of inter-story drift ratio of each floor in the X and Y-direction are plotted in Fig. 12. The responses under one direction and bidirection loading are shown in Fig. 12(a) and (b), respectively. It is noted that the displacement response under bi-direction loading is larger than one direction loading. The displacement response of X-direction is generally larger than Y-direction.

Under SLE level input (PGA = 0.14 g), the 3rd floor (roof) showed the largest inter-story drift with the value of 0.12%–0.2% and 0.1%–0.15% in X-direction and Y-direction, respectively. As the input PGA increased to 0.4 g, the 2nd floor showed the largest inter-story drift. The maximum inter-story drift was 0.5% and 0.25% in X-direction and Y-direction, respectively. It indicated that the sliding mechanism was triggered in the DBE level input.



Fig. 9. Damage observations of the test model.

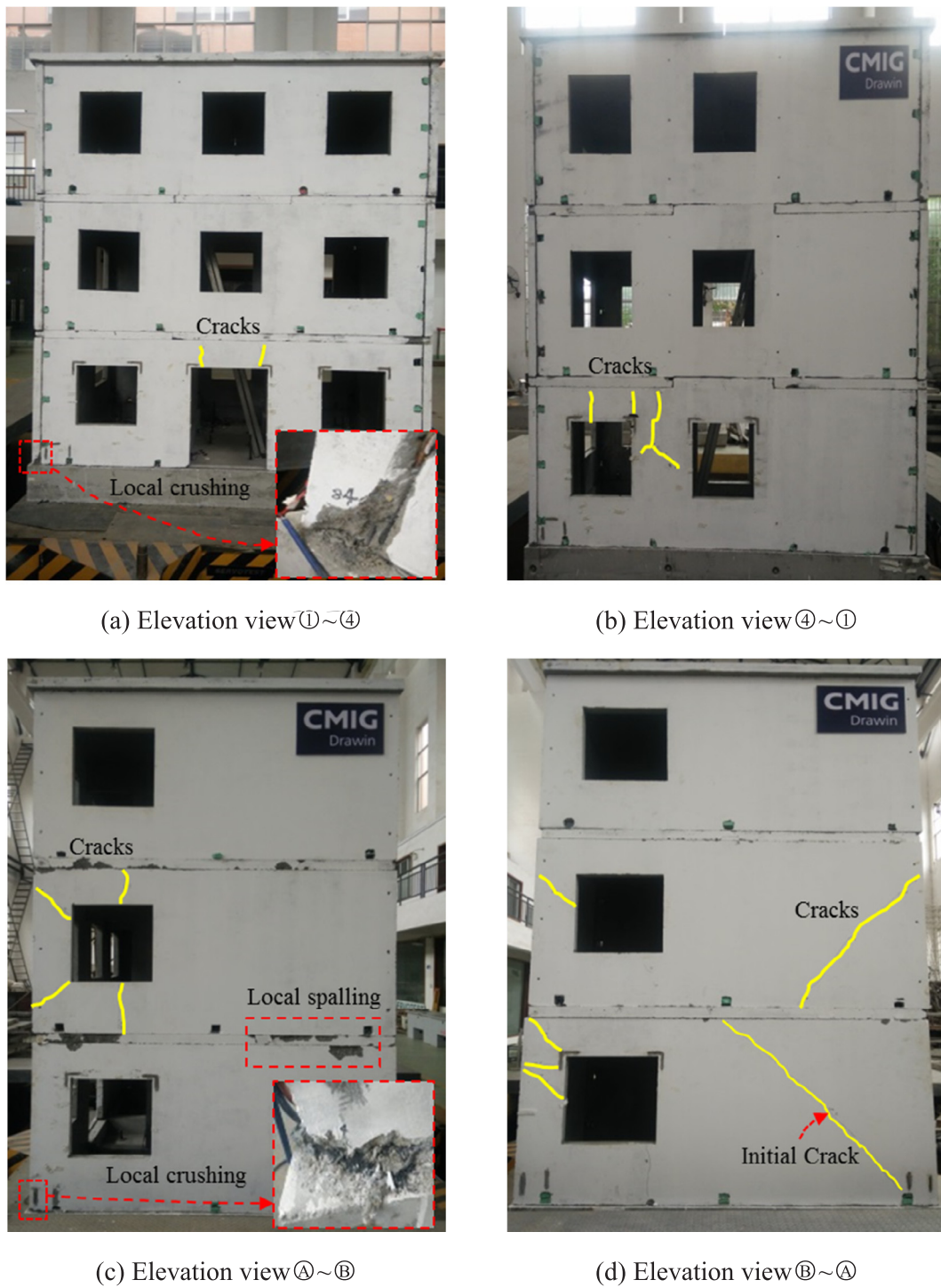


Fig. 10. Overall damage and crack distribution of test model.

Table 4
Natural frequencies of test model before retightening the bolts.

Modal order	Before test (initial state)	After SLE test		After DBE test	
		Frequency (Hz)	Degradation ratio	Frequency (Hz)	Degradation ratio
1st	11.154	11.139	1.3%	9.995	10.4%
2nd	11.688	11.124	4.8%	10.391	11.1%

Table 5
Natural frequencies of test model after retightening the bolts.

Modal order	Bolt tightened before MCE	After MCE test	
		Frequency (Hz)	Degradation ratio
1st	15.366	12.360	19.6%
2nd	16.632	13.596	18.3%

Under MCE level input (PGA = 0.8 g), the displacement response of specimens was different between the one direction loading and bi-direction loading. In the one direction loading cases, the maximum inter-story drift was around 8% and 5% in X-direction and Y-direction, respectively. While in the bi-direction loading cases, the maximum inter-story drift was concentrated in the 1st story and increased to around 8% in both directions.

As discussed above, the sliding of floor slab leads to the amplification of acceleration responses of the first and second floor. Similarly, the displacement response increases while floor slabs slide. In general, the inter-story drift of the first and second floor is greater than that of third floor in both X and Y-direction for the DBE and MCE level input. It is consistent with the test phenomena of sliding at the first and second floor slab. It means the lateral deformation mode of test structure is dominated by sliding of shear wall, instead of bending deformation of cast-in-situ shear wall structure.

4.5. Inter-story drift components

The inter-story drift is composed of sliding displacement and shear wall lateral deformation, as shown in Fig. 13. Measured time histories

of the inter-story drift Δ and the corresponding dislocation displacement d_1 , d_2 and wall deformation d_3 under Y-direction input of MCE level excitation (one direction loading) are plotted in Fig. 14. Before MCE level excitations, the bolts are tightened. There is almost no residual displacement under Kobe excitation. The components remain elastic. Under Manjil Iran and Whittier Narrows excitations, residual displacement of Δ increases obviously. By comparison, it can be found that there is almost no wall residual deformation. The residual displacement of Δ is cause by sliding displacement d_1 , d_2 . On the whole, d_1 does the largest contribution to Δ . The maximum Δ , d_1 , d_2 and d_3 are depicted and compared in Fig. 15. It is observed that d_1 is larger than d_2 and d_3 , and it even larger than Δ in artificial and Manjil Iran excitations. The contribution of the sliding between the 1st story and foundation is the primary contribution to the 1st story drift. The lateral deformation of the precast wall is therefore relatively small. To evaluate the seismic performance of the LPWSBC system, both the sliding displacement and the lateral deformation of the precast wall should be separated.

4.5.1. Floor slab sliding

In LPWSBC structural system, the shear walls are connected by the bolt connections. As observed in the test, the floor sliding has a significant influence on the stiffness and performance of specimen. The main reasons for the floor slab sliding are as follows: (a) large acceleration response causes rapid and dynamic tension cycle of bolt connections, and this cycle isn't considered in design process and would cause the loss of pre-tightening force; (b) the constraints of bolt connections is weak because of no concrete to fill the hollows around the bolt connections in the test model; (c) the friction force of the precast component interface is relatively small due to the small axial load ratio (approximately 0.0036) of the specimen, so the floor slabs slide in the

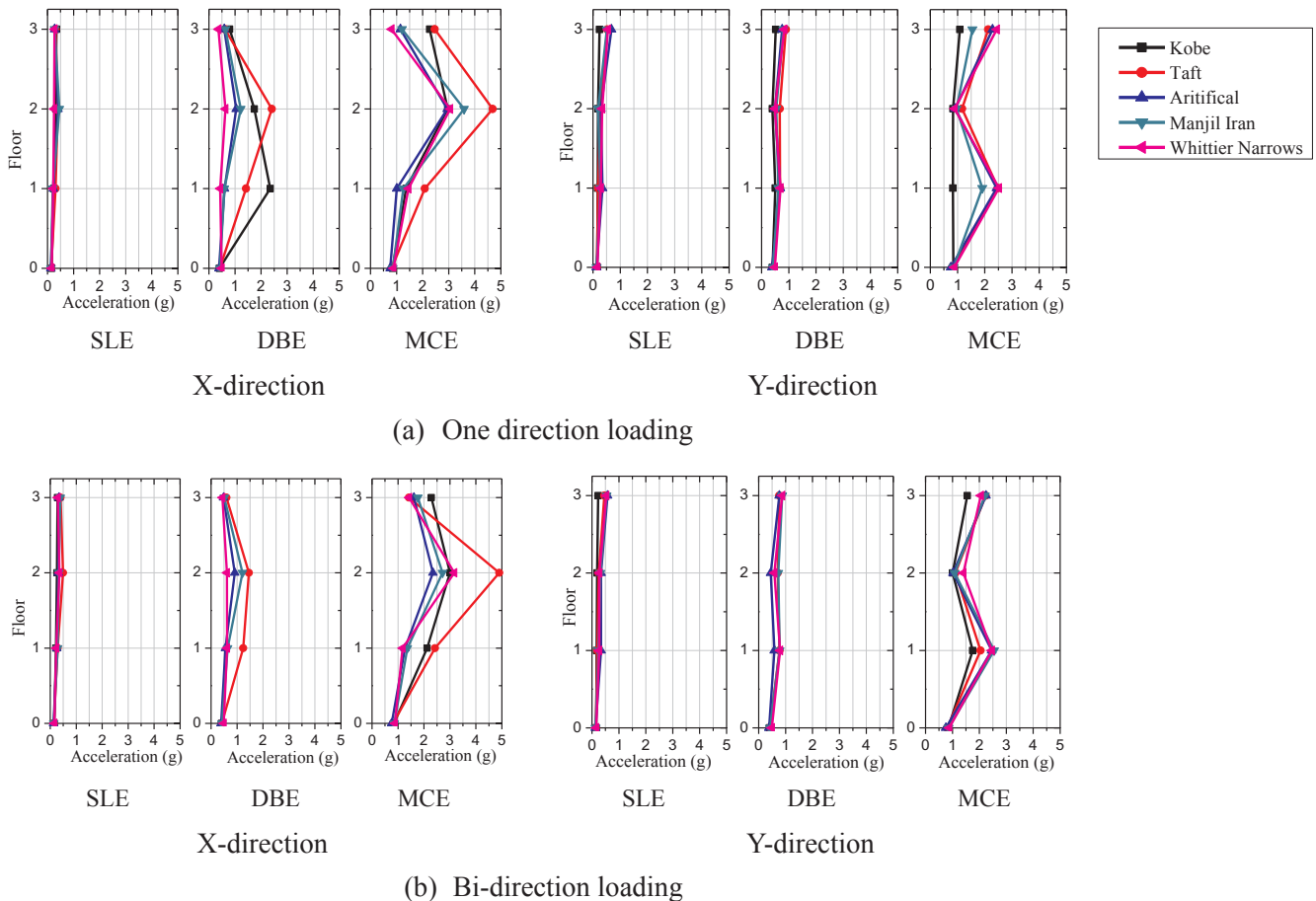


Fig. 11. Envelope diagram of acceleration responses.

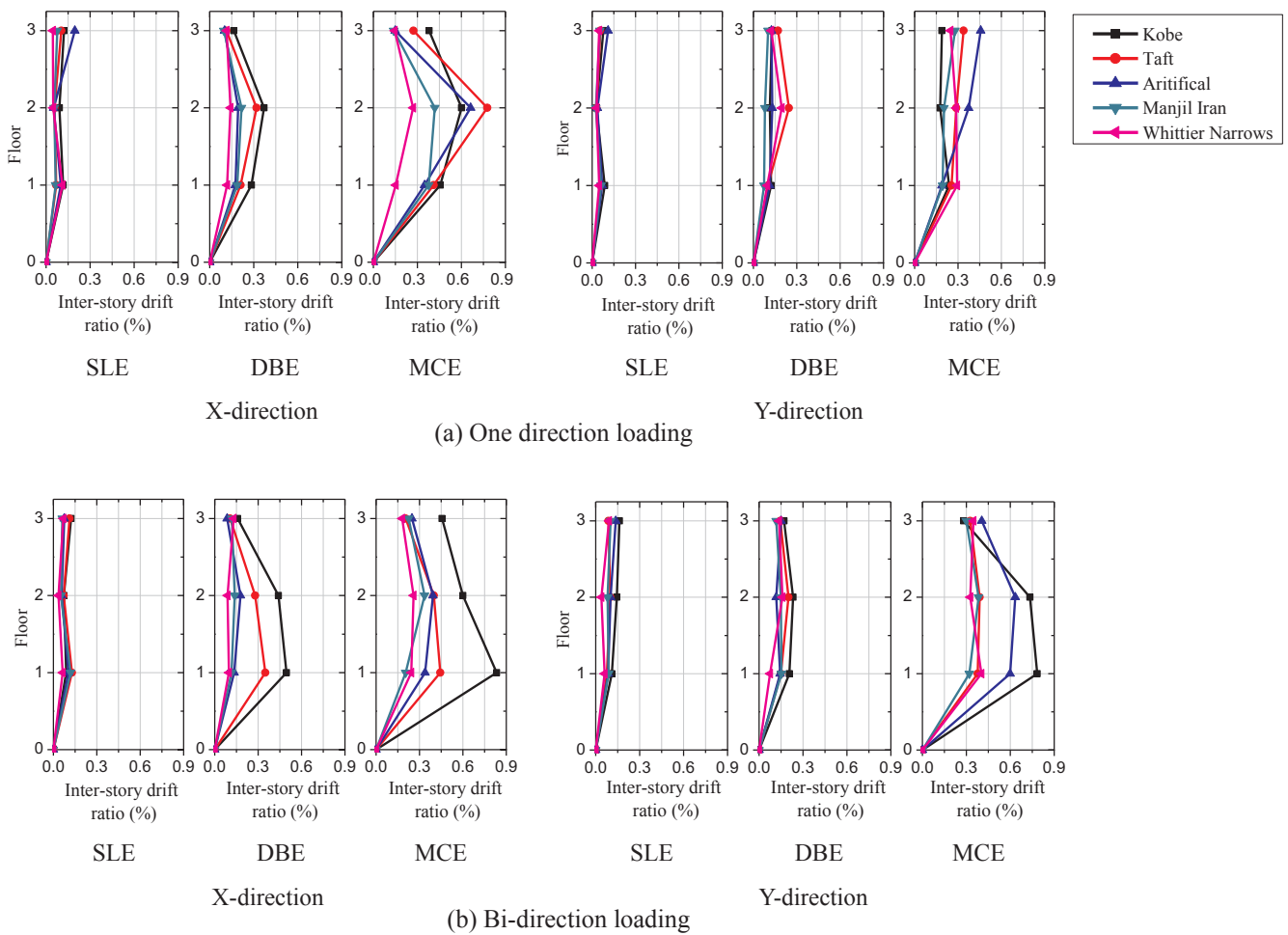


Fig. 12. Envelope diagram of inter-story drift ratio.

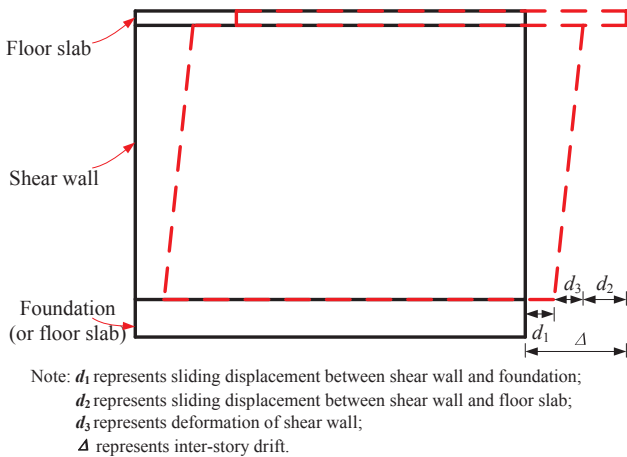


Fig. 13. The components of inter-story drift.

early loading stage. As the primary lateral resistance component, the dry connections have a significant influence on the dynamic characteristics and responses of the structure. Considering the floor slab sliding may cause severe damage to fixtures and non-structural components, it is necessary to control the floor slab sliding values by several measures, such as increasing the number of dry connections, increasing the pre-tension force of the high strength bolts.

4.5.2. Lateral deformation of precast wall

Under the DBE level excitation, measured peak strains of the rebars are less than $2000 \mu\epsilon$. It indicated that the components were not yielded or slightly yielded. Under MCE level excitation, the measured strain of several rebars around the dry connection part exceed the yield strain with the maximum strain less than $3000 \mu\epsilon$. Moreover, the longitudinal rebar of the precast walls were not yielded. It indicated that the damage of the precast wall is slight and the damage of the specimen is mainly concentrated by the floor sliding.

As observed from the test, the shear wall lateral deformation of LPWSBC is dominated by translational sliding, which is different from the traditional cast-in-situ concrete structure. Therefore, it is inappropriate to adopt the code given limit value of inter-story drift ratio to evaluate the damage state of LPWSBC. The sliding displacement and deformation of shear wall should be separated and analyzed respectively. To evaluate the damage of shear wall, the shear wall deformations are calculated by the test results and the corresponding values of prototype structure are also given. Fig. 16 shows the maximum deformation of shear walls. Because the Y-direction is analyzed to be weak axis before the test, the deformation of wall SW1-1 and SW4-1 are measured. The Chinese code [37] also gives the deformation limit value of inter-story drift ratio: the inter-story drift ratio for the performance level of no damage under SLE is 1/1000, and the inter-story drift ratio for the performance level of collapse prevention correspond to 1/120. Then by multiplying the height of shear wall, the deformation limit values for no damage and collapse prevention are 2.55 mm and 21.25 mm, respectively.

In Fig. 16, the mean value of wall deformations is 2.44 mm for SLE

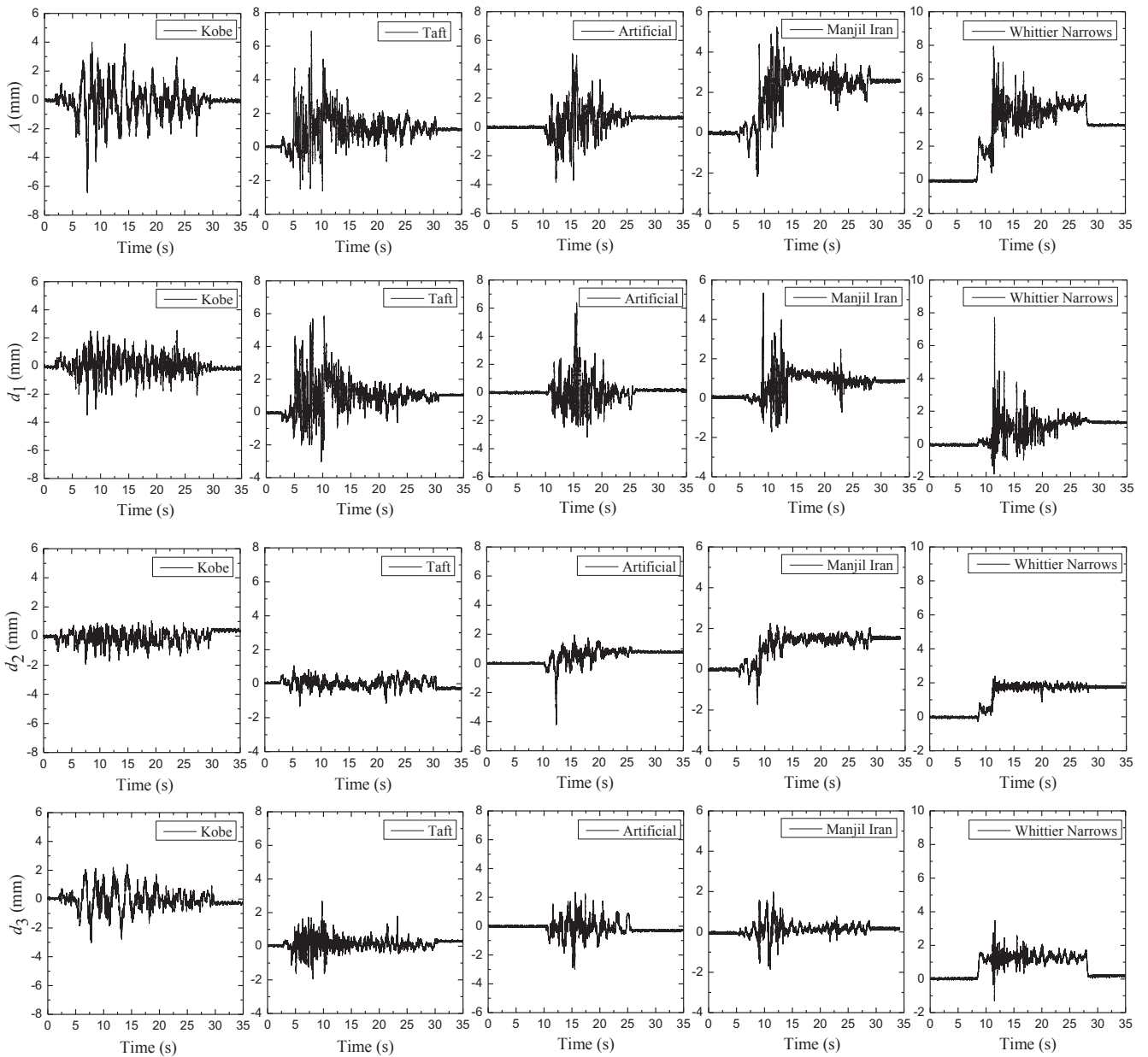


Fig. 14. Time history curves of Δ at the first floor under Y direction input of MCE level excitation and the corresponding d_1 , d_2 and d_3 .

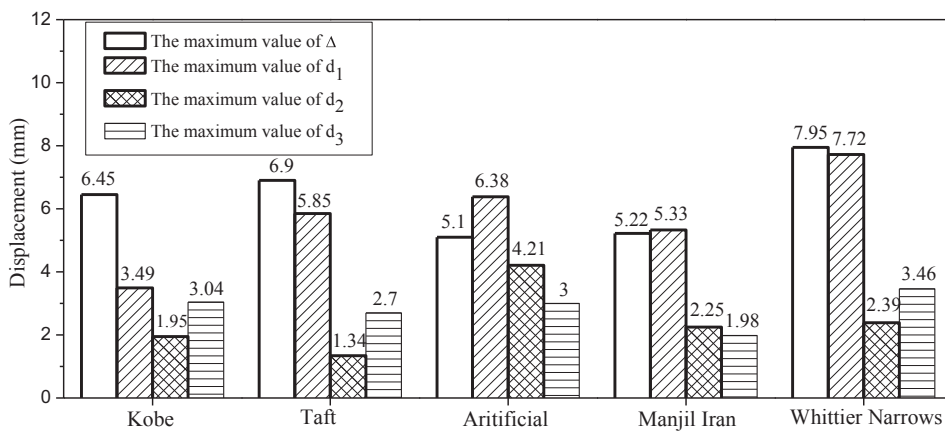


Fig. 15. The maximum value of Δ , d_1 , d_2 and d_3 at the first floor under Y direction input of MCE level excitation.

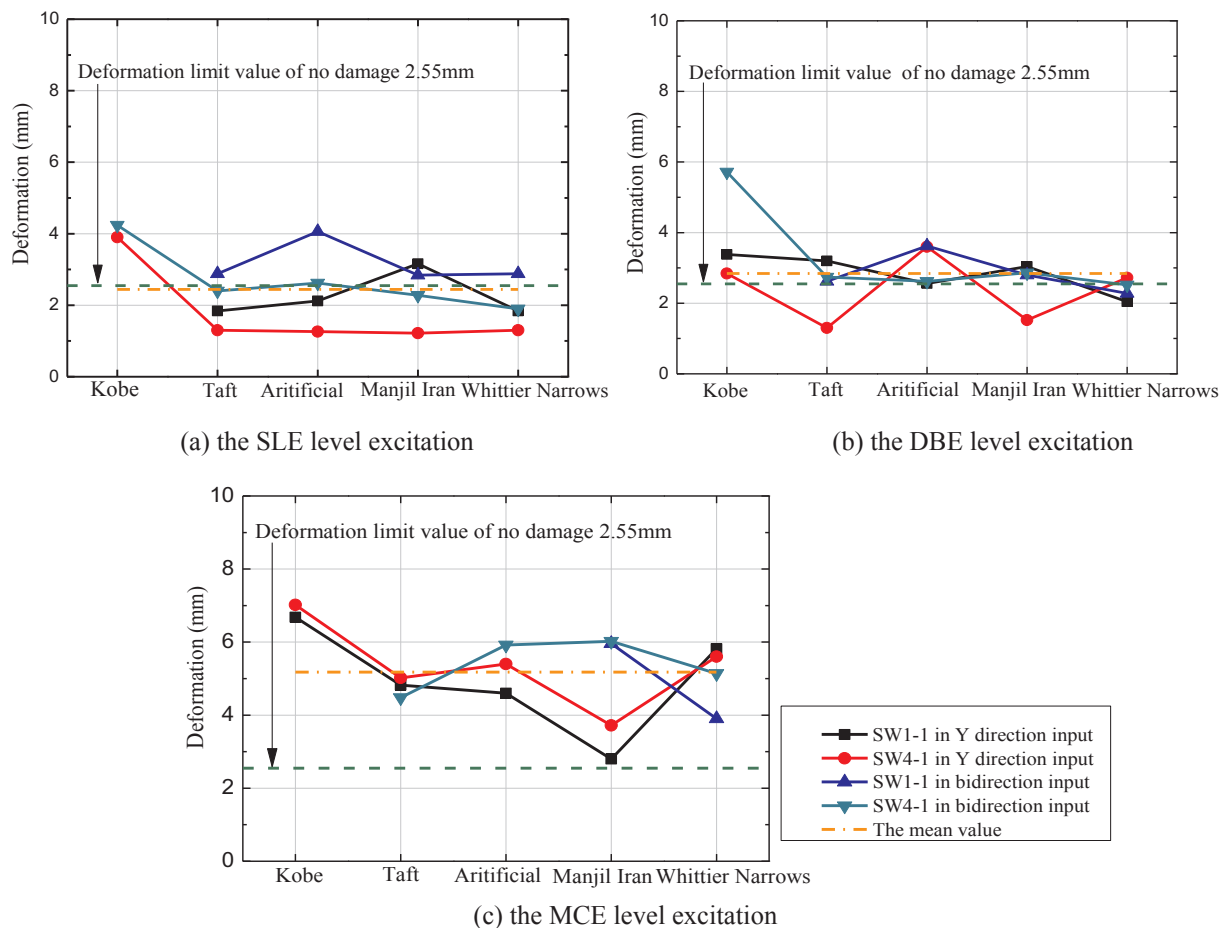


Fig. 16. Maximum lateral deformation of precast walls.

level excitation, which is less than the limit value of no damage 2.55 mm. The structure is in the elastic state according to the test observations. The mean value of wall deformation for DBE level excitation is 2.84 mm, which is slightly larger than the 2.55 mm. For MCE level excitation, the mean value of wall deformation increases to 5.18 mm, which is much smaller than the collapse prevention limit. The above analysis is generally in accord with the wall damages described in Section 4.1.

5. Development of fragility for LPWSBC

In the next-generation seismic performance assessment of buildings (e.g., FEMA P-58 [40]), performance is expressed as the probable consequences in terms of direct economic losses, require time and other metrics associated with a certain intensity of ground motion shaking. A fundamental component for performance assessment is the reliable fragility functions, which are the estimation of damage in a structural component for a given engineering demand parameter. Since the structural safety is the primary concern of this study, the fragility is defined based on structural damage, and the wall drift ratio is adopted as the engineering demand parameter based on the test observation and data. Although the floor sliding could cause severe damage to fixtures and non-structural components in the presented structure system, the relationship between damage state of non-structural components and engineering demand parameters, such as the floor sliding displacement, is unclear for developing the fragility. Previous studies [41,42] provided a reference to seismic fragility of cast-in-place building considering structural and non-structural components. However, it may not be appropriate for the new structure system presented in this paper. Hence, damage state of non-structural components is not considered in

this section.

5.1. Performance objectives

The LPWSBC structural system in this paper differs from traditional cast-in-suit structure, and its dynamic responses and damage are related with the bolt connection. According to the test observations and analysis, the performance design objective of the LPWSBC can be given: (a) for SLE, allowing the bolt loosening and structural components remain elastic; (b) for DBE, allowing the floor slabs slide obviously, and structural components suffer slight damages, such as local concrete crack and spall; (c) for MCE, allowing structural components moderate or serious damage, and collapse induced by slab slide and wall deformation should be prevented. The structural performance level is determined by performance of wall and bolt connection. According to the test observations, the wall damage is more serious compared with the bolt connection. Therefore, the drift ratio of shear wall is adopted as the evaluation index for structural performance level. The seismic intensity and corresponding performance objective are summarized in Fig. 17. The structural performance levels and the inter-story drift ratio thresholds will be specified in Section 5.2.

5.2. Damage limit states

The definition of damage limit is an important step for fragility analysis. The structural seismic performance can usually be evaluated through four damage limit states, for instance, LS1: no damage, LS2: minor structural damage and moderate non-structural damage, LS3: significant structural damage and extensive non-structural damage, LS4: severe damage leading to demolition [43]. After the qualitative

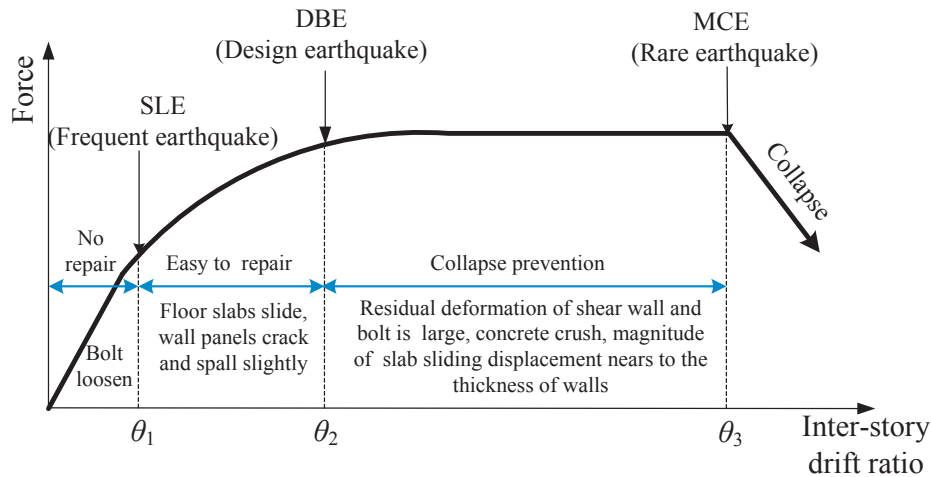


Fig. 17. Performance objective of the LPWSBC structural system.

description of the damage limit state, it is necessary to select the index of engineering parameters to quantitatively express the damage. The inter-story drift ratio is a common quantitative index. Nazari [44] pointed out that the first-story drift can be adopted to quantify the damage state of the concrete shear wall structure. The NHERP [45] and ASCE 41 [46] suggested that the drift ratio for the limit state of immediate occupancy, life safety and collapse prevention is 0.5%, 1% and 2%, respectively. The Chinese code [47] is more conservatively to suggest that the drift ratios for limit state of no damage and collapse prevention are 1/1000 and 1/120, respectively. As mentioned in Section 5.1, the drift ratio of shear wall is adopted as the evaluation index of the damage limit states. And four damage limit states are used to describe the structure performance levels.

LS1 implies that the structure components remain elastic and allows the bolt loosening. It can be used normally without repair. The corresponding performance level is defined as operational (OP). In the test observations after SLE, no obvious structural damage was found, but only the bolt loosening. Repair isn't needed for the structure. According to the Section 4.5.2, the median deformation of shear walls is 2.44 mm, and the corresponding wall drift ratio is 1/1045. Combined with Chinese code, 1/1000 is suggested as the limit value for this damage state.

LS2 means that the structural damage is slight and easy to repair. The corresponding performance level is defined as immediate occupancy (IO). Based on the test observations and result analysis, the structural damages after MCE is coincide with this performance level. The median deformation of shear walls for MCE is 5.18 mm, and the corresponding wall drift ratio is 1/492. Hence, 1/500 is suggested as the limit value for this damage state.

LS3 implies the structure appears moderate damage, the property and life safety is threatened. Structural function should be restored by repair and treatment. LS4 means the structure nears to partial or complete collapse. The corresponding performance levels for LS3 and LS4 are defined as life safety (LS) and collapse prevention (CP), respectively.

As discussed in Section 4.6.2, the limit value of drift ratio for LS4 is proposed as 1/120. To further illustrate, Fig. 18 draws the backbone curve of a shear wall of LPWSBC by quasi-static test. This test is carried out at Central South University [47]. Dash line in this figure represents equivalent bilinear model based on equal energy criterion. According to the quasi-static test, the bolt connection was broken, and concrete in the compression zone was crushed in failure state of the wall. The drift ratio of failure state is 1/113, which demonstrates the rationality that wall drift ratio for LS4 adopts 1/120. In generally, the drift ratio of yield point can be used as the evaluation index for slight damage state (LS2). The drift ratio of yield point based on equivalent bilinear model is 1/555, that is approximate to the 1/500 suggested for LS2. For LS3, the

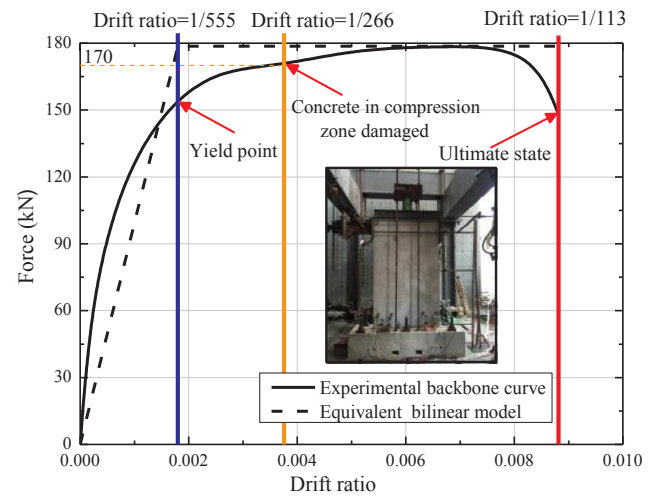


Fig. 18. Backbone curve of a shear wall acquired by quasi-static test.

limit value of drift ratio should be in the range between 1/500 and 1/120. According to the quasi-static test, the concrete in compression zone began to be crushed under 170kN lateral force. Then the development of wall damages accelerated. And the damages need repair and treatment. The drift ratio corresponding to 170kN lateral force is 1/266. Hence, it suggests that the drift ratio threshold for LS3 adopts 1/270. In conclusion, the limit value for LS3 and LS4 is 1/270 and 1/120, respectively. The limit states and the corresponding performance levels are summarized in Table 6.

6. Seismic fragility for prototype structure

Seismic fragility analysis is an important approach to evaluate the seismic performance of structures. It can predict the probability of each damage state occurring under different seismic level. In the previous study, many scholars have carried out shaking table test to assess the fragility for building components [48–51]. Due to the damage progressive accumulation in shaking table test, it is often difficult to obtain the structural fragility curves. Graziotti [48] conducted a shaking table test on two-story full scale unreinforced masonry, and given the damage limit states as well as the corresponding inter-story drift ratio threshold. Because of the progressive accumulation of damage, the structural fragility curves didn't be obtained. Mendes [49] obtained the fragility curve of a masonry building based on the decrease of natural frequencies that was obtained through test. To a certain extent, this

Table 6
The definition of limit states for each performance level.

Limit state	Description of damage		Performance objective	Performance level	Wall drift ratio threshold
	Bolt connection	Wall			
LS1	Loosening	No structural damage	No repair	OP	1/1000
LS2	No obvious damage	Few cracks, local slight spalling and walls dislocate	Easy to repair	IO	1/500
LS3	Yield obviously	Yield obviously, and serious local damage.	Need repair and treatment	LS	1/270
LS4	Large residual deformation, or broken by tension-shear force	Concrete in wall compression zone crush completely, and residual deformation is large	Collapse prevention	CP	1/120

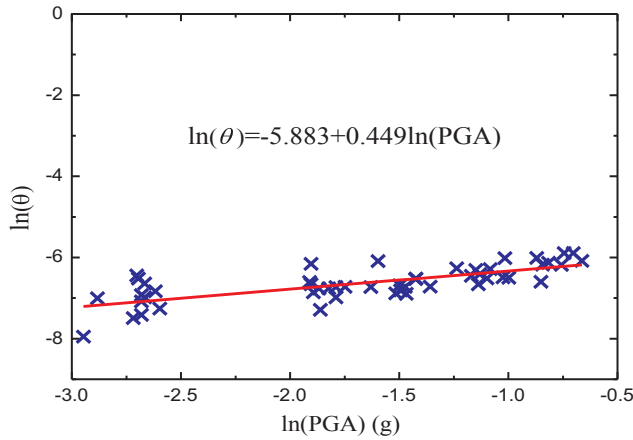


Fig. 19. Linear regression for θ of prototype structure.

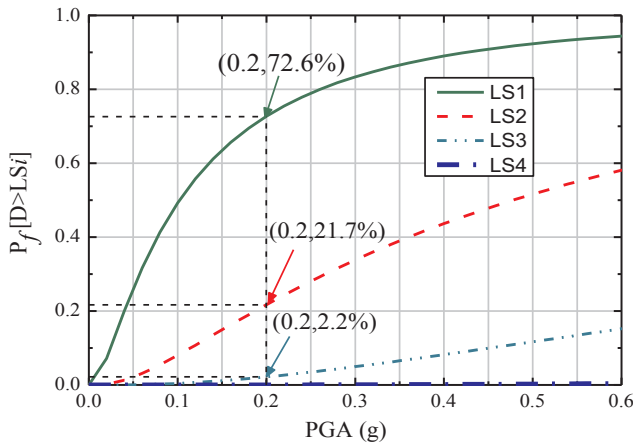


Fig. 20. Fragility curves for prototype structure.

fragility curve reflected the relationship between structure damage level and seismic intensity. However, it cannot obtain the failure probability of each damage state. Cosenza [50] derived fragility curves for nonstructural components by a systemic approach with less test samples [51]. This fragility curves can effectively assess the fragility of nonstructural components. In the test performed by Cosenza [50], the different components were relocated in their original condition after each loading case. Hence, there is no damage progressive accumulation. In the test of this study, the observations and results have shown that the overall damage of the structure is slight, and yield behavior of the structure is not obvious. Therefore, the influence of accumulative damage can be ignored during the functional relationship between engineering demand parameters and ground motion intensity is established.

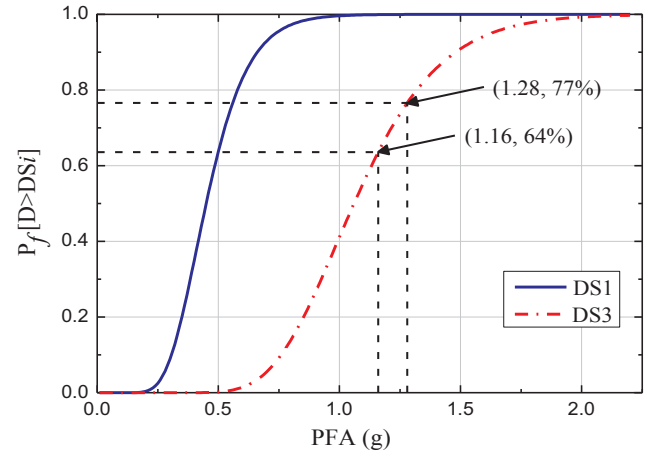


Fig. 21. Fragility curves for nonstructural components.

6.1. Fragility of the structure

In seismic fragility analysis, the structural loading capacity and seismic response are considered as normal distribution. The relation between engineering demand parameter (*EDP*) and ground motion intensity measure (*IM*) is deemed as exponential distribution, that is:

$$EDP = \alpha (IM)^\beta \tag{5}$$

where α and β are unknown regression coefficients obtained from logarithm linear regression. Fragility function that gives the probability of exceeding predefined performance level under different ground motion intensity can be given by [51]:

$$P_f [D > LSi | IM] = \Phi \left[\frac{\ln(D/C)}{\sqrt{\beta_c^2 + \beta_d^2}} \right] \tag{6}$$

where D and C are the mean values of *EDP* and capacity variable, respectively. C can be obtained from Table 6 for each damage limit state. β_c and β_d are the logarithmic standard deviations for D and C . According to HAZUS99 [52], $\sqrt{\beta_c^2 + \beta_d^2}$ can be selected as 0.5 when *PGA* is adopted as *IM*.

In this paper, the drift ratio of shear wall θ is adopted as *EDP*. In the test, the deformation of wall SW1-1 and SW4-1 were measured. Only the test cases with Y-direction and bidirectional direction input are considered because of displacement sensors are only installed in the Y-direction. The θ for each case is the mean value of wall SW1-1 and SW4-1. According to the similarity relationships, the θ for prototype structure can be calculated. Similarly, *IM* (*PGA*) for prototype structure also can be calculated based on the measured acceleration on the shaking table. According Eq. (1), the relation between θ and *IM* can be expressed as:

$$\ln(\theta) = \ln \alpha + \beta \ln(PGA) = a + b \ln(PGA) \tag{7}$$

where a and b can be obtained from logarithm linear regression, the

Table 7
Peak floor acceleration (PFA) of prototype structure and corresponding exceeding probability.

Floor number	PFA under DBE	$P_f [D > DS1]$	$P_f [D > DS3]$	PFA under MCE	$P_f [D > DS1]$	$P_f [D > DS3]$
1	1.16 g	1	0.64	1.28 g	1	0.77
2	1.16 g	1	0.64	2.58 g	1	1

result is displayed in Fig. 19. By substituting linear regression equation into Eq. (6), the fragility curves for each the damage limit state can be obtained, as shown in Fig. 20.

According to Fig. 20, the probabilities of exceeding LS1, LS2, LS3 and LS4 are 72.6%, 21.7%, 2.2% and 0 under the excitation of DBE (PGA = 0.2 g for prototype structure), respectively. This predicts that slight damage under the DBE is likely to happen, and the structural collapse will not occur. Under the seismic level of MCE (PGA = 0.4 g), the probabilities of exceeding LS3 and LS4 are 8.2% and 0.1%. Even the PGA increases 0.6 g, the probability of exceeding LS3 and LS4 is only 15.2% and 0.4%, respectively. Namely, the probability of moderate damage or collapse occurred is very small even in high seismic intensity. This indicates that the structure has high loading capacity and high collapse margin ratio. Its seismic performance is commendable.

6.2. Fragility of acceleration-sensitive nonstructural components

In view of that the damages of nonstructural components usually lead to more financial loss than structural components. And the large acceleration responses of the structure proposed in this paper may cause damage to the nonstructural components. The fragility of acceleration sensitive equipments will be preliminarily analyzed at here. Cosenza [50] has obtained fragility curves of some acceleration sensitive equipments by shanking table test, as shown in Fig. 21. The horizontal axis in this figure represents peak floor acceleration (PFA), and the vertical axis represents exceeding probability of each damage limit state. Three damage states are defined by Cosenza [50], as following: DS1: operational interruption; DS2: need to replace damaged part of the components; DS3: need to replace the whole component or threat for life safety. For DS2, there is no fragility curve available. The PFA of prototype structure in this paper is listed in Table 7. The third floor is not considered because its acceleration responses are relatively smaller. Under DBE excitations, the exceeding probabilities of DS1 and DS3 for each floor are 100% and 64%, respectively. The exceeding probabilities of DS1 are both 100% under MCE excitations, and exceeding probabilities of DS3 are 77% and 100%, respectively. Hence, it's deemed that the nonstructural components are likely to be replaced and cause economic loss. Considering the PFA is related to the wall sliding and floor slab dislocation after bolt loosening, the joint connections need to be further ameliorated to reduce the structural acceleration responses.

7. Conclusions

This paper introduces a new precast structure system (LPWSBC) with a very rapid assembly advantage. The dynamic characteristics, dynamic responses and damage pattern of the LPWSBC are analyzed by a shaking table test of half scaled model. The performance design objectives are proposed based on the test results, and seismic fragility of the prototype structure are performed via the experimental results. The following conclusions are obtained:

- (1) The high strength bolt connections play a decisive role in the structural initial stiffness and have a significant effect on structure dynamic responses. It's the primary lateral resistance component. Although bolt of the connections loosened under seismic excitation, the steel plates didn't yield and only few anchored rods appeared slight residual deformation. The joint connections are reliable.
- (2) Tensile or shear cracks began to appear after DBE level excitation,

and mainly distributed around the opening. Damage pattern of the structure followed the sequence of high strength bolts loosening, adjoining wall panels sliding and dislocating, structural components cracking. On the whole, the structural damage is slight. According to the analysis of dynamic responses, most of the structural components remained elastic. The overall stiffness of the structure is high and the seismic performance is good.

- (3) The sliding of floor slab is significant, especially at first and second floor. By analyzing the inter-story drift components, it reveals that the contribution of the slab sliding is the primary contribution to the inter-story drift. And the lateral deformation of the precast wall is relatively small.
- (4) Combined with the experimental phenomenon and measured values of wall deformation, the performance design objectives for SLE, DBE and MCE are given, and four damage limit states are defined. Then fragility curves of the prototype structure for each damage limit state are derived. The result shows that probability of structure collapse approximately to be zero under the seismic level of MCE. The structure has high loading capacity and high collapse margin ratio.
- (5) According to the fragility evaluation of nonstructural components, acceleration response of the structure is likely to cause economic loss. Considering the stiffness, loading capacity and collapse margin ratio of the structure is high, it is suggested that the bolt connections should be ameliorated and the structural system should be optimized to reduce the structural acceleration responses.

Acknowledgements

The authors are grateful for the financial support from the Fundamental Research Funds for the Central Universities of Central South University (Project No. 502221804), the National Natural Science Foundation of China (Project No. 51878674, 51678106), the Foundation for Key Youth Scholars in Hunan Province and the Project of Yuying Plan in Central South University. Any opinions, findings, and conclusions or recommendations expressed in this paper are those of the authors.

References

- [1] Lachimpadi SK, Pereira JJ, Taha MR, et al. Construction waste minimisation comparing conventional and precast construction (Mixed System and IBS) methods in high-rise buildings: a Malaysia case study. *Resour Conserv Recycl* 2012;68(4):96–103.
- [2] Dong YH, Jaillon L, Chu P, et al. Comparing carbon emissions of precast and cast-in-situ construction methods – a case study of high-rise private building. *Constr Build Mater* 2015;99:39–53.
- [3] Ioani AM, Tripa E. Structural behavior of an innovative all-precast concrete dual system for residential buildings. *PCI J* 2012;57(1):110–23.
- [4] Brunesi E, Nascimbene R. Experimental and numerical investigation of the seismic response of precast wall connections. *Bull Earthq Eng* 2017;5:1–40.
- [5] Vaghei R, Hejazi F, Taheri H, et al. Evaluate performance of precast concrete wall to wall connection. *APCBEE Procedia* 2014;9(9):285–90.
- [6] Xu G, Wang Z, Wu B, et al. Seismic performance of precast shear wall with sleeves connection based on experimental and numerical studies. *Eng Struct* 2017;150:346–58.
- [7] Lago BD, Biondini F, Toniolo G. Friction-based dissipative devices for precast concrete panels. *Eng Struct* 2017;147:356–71.
- [8] Pavese A, Bournas DA. Experimental assessment of the seismic performance of a prefabricated concrete structural wall system. *Eng Struct* 2011;33(6):2049–62.
- [9] Todut C, Dan D, Stoian V. Theoretical and experimental study on precast reinforced concrete wall panels subjected to shear force. *Eng Struct* 2014;80:323–38.
- [10] Kurama Y, Pessiki S, Sause R, et al. Seismic behavior and design of unbonded post-tensioned precast concrete walls. *Pci J* 1999;44(3):72–89.

- [11] Perez FJ, Sause R, Pessiki S, et al. Lateral load behavior of unbonded post-tensioned precast concrete walls. *Adv. Build Technol* 2002;49(2):423–30.
- [12] Nurjaman H, Faizal L, Sidjabat H, et al. Application of precast system buildings with using connection of unbonded post-tension and local dissipater device. *Procedia Eng* 2014;95:75–87.
- [13] Rassouli B, Shafaei S, Ayazi A, et al. Experimental and numerical study on steel-concrete composite shear wall using light-weight concrete. *J Constr Steel Res* 2016;126:117–28.
- [14] Zhi Q, Guo Z, Xiao Q, et al. Quasi-static test and strut-and-tie modeling of precast concrete shear walls with grouted lap-spliced connections. *Constr Build Mater* 2017;150:190–203.
- [15] Chai YH, Anderson JD. Seismic response of perforated lightweight aggregate concrete wall panels for low-rise modular classrooms. *Eng Struct* 2005;27(4):593–604.
- [16] Amran YHM, Ali AAA, Rashid RSM, et al. Structural behavior of axially loaded precast foamed concrete sandwich panels. *Constr Build Mater* 2016;107:307–20.
- [17] Brunesi E, Nascimbene R, Pavese A. Mechanical model for seismic response assessment of lightly reinforced concrete walls. *Earthquakes Struct* 2016;11(3):461–81.
- [18] Ricci Ilaria, Palermo M, et al. Results of pseudo-static tests with cyclic horizontal load on cast in situ sandwich squat concrete walls. *Eng Struct* 2013;54(3):131–49.
- [19] Liu R, Pantelides CP. Shear strength of GFRP reinforced precast lightweight concrete panels. *Constr Build Mater* 2013;48(11):51–8.
- [20] Yu ZW, Liu HY, Guo W, Liu Q. A general spectral difference method for calculating the minimum safety distance to avoid the pounding of adjacent structures during earthquakes. *Eng Struct* 2017;150:646–55.
- [21] Gu Q, Liu YD, Guo W, Li WQ. A practical wheel-rail interaction element for modeling vehicle-track-bridge systems. *Int J Struct Stab Dyn* 2019;19(2):195001.
- [22] Hou WQ, Li YK, Guo W, Li JL, Chen YH, Duan XX. Railway vehicle induced vibration energy harvesting and saving of rail transit segmental prefabricated and assembling bridges. *J Cleaner Prod* 2018. <https://doi.org/10.1016/j.jclepro.2018.02.019>.
- [23] Guo W, Wu J, Hu Y, Li YS, Yang TY. Seismic performance evaluation of typical dampers designed by Chinese Building Code. *Earthquake Eng Eng Vibrat* 2019. (accepted for publication).
- [24] Gou HY, Yang LC, Leng D, Bao Y, Pu Q H. Effect of bridge lateral deformation on track geometry of high-speed railway. *Steel Compos. Struct.* 2018:accepted.
- [25] Gou HY, He YN, Zhou W, Bao Y, Chen GD. Experimental and numerical investigations of the dynamic responses of an asymmetrical arch railway bridge. *P. I. Mech. Eng. F-J. RAI* 2018. <https://doi.org/10.1177/0954409718766929>.
- [26] Gou HY, Zhou W, Chen GD, Bao Y, Pu QH. In-situ test and dynamic analysis of a double-deck tied-arch bridge. *Steel Compos. Struct.* 2018;27(1):161–75.
- [27] Gou HY, Long H, Bao Y, Chen GD, Pu QH, Kang R. Experimental and numerical studies on stress distributions in girder-arch-pier connections of long-span continuous rigid frame arch railway bridge. *J. Bridge Eng.* 2018;23(7):04018039.
- [28] Gou HY, Wang W, Shi XY, Pu QH, Kang R. Behavior of steel-concrete composite cable anchorage system. *Steel Compos. Struct.* 2018;26(1):115–23.
- [29] Gou HY, Shi XY, Zhou W, Cui K, Pu QH. Dynamic performance of continuous railway bridges: numerical analyses and field tests. *P. I. Mech. Eng. F-J. RAI* 2018;232(3):936–55.
- [30] Gavridou S. Shake table testing and analytical modeling of a full-scale, four-story unbonded post-tensioned concrete wall building. *Dissertations and Theses-Gradworks*. 2015.
- [31] Lim WY, Kang HK, Hong SG. Cyclic lateral testing of precast concrete T-walls in fast low-rise construction. *ACI Struct J* 2016;113(1):179–89.
- [32] Lago BD, Muhaxheri M, Ferrara L. Numerical and experimental analysis of an innovative lightweight precast concrete wall. *Eng Struct* 2017;137:204–22.
- [33] Henry RS, Aaleti S, Sritharan S, et al. Concept and finite-element modeling of new steel shear connectors for self-centering wall systems. *J Eng Mech* 2010;11(2):220–9.
- [34] Bournas DA, Negro P, Molina FJ. Pseudodynamic tests on a full-scale 3-storey precast concrete building: behavior of the mechanical connections and floor diaphragms. *Eng Struct* 2013;57(4):609–27.
- [35] Negro P, Bournas DA, Molina FJ. Pseudodynamic tests on a full-scale 3-storey precast concrete building: global response. *Eng Struct* 2013;57(4):594–608.
- [36] Bora C, Oliva MG, Nakaki SD, et al. Development of a precast concrete shear-wall system requiring special code acceptance. *Pci J* 2007;52(1):122–35.
- [37] GB 50011-2010. Code for seismic design of buildings. Beijing: China Architecture and Industry Press; 2010. (in Chinese).
- [38] GB 50011-2010. Code for seismic design of buildings. Beijing: China Architecture and Industry Press; 2010. (in Chinese).
- [39] GB 50017-2010. Code for design of concrete structures. Beijing: China Architecture and Industry Press; 2010. (in Chinese).
- [40] FEMA. Seismic performance assessment of buildings Volume 1—methodology. Washington D C: Federal Emergency Management Agency; 2012.
- [41] Applied Technology Council (ATC). Seismic Performance Assessment of Buildings, Volumes 1 and 2, Report No. ATC-58, Redwood City, CA. 2012.
- [42] Yang TY, Atkinson JC, Tobber L. Detailed seismic performance assessment of high-value-contents laboratory facility. *Earthquake Spectra* 2015;4(31):2117–35.
- [43] Calvi GM. A displacement-based approach for vulnerability evaluation of classes of buildings. *J Earthquake Eng* 1999;3(3):411–38.
- [44] Nazari YR, Saatcioglu M. Seismic vulnerability assessment of concrete shear wall buildings through fragility analysis. *J Build Eng* 2017.
- [45] FEMA-273. NEHRP guidelines for the seismic rehabilitation of buildings. FEMA-273. Washington, DC: Federal Emergency Management Agency; 1997.
- [46] ASCE. Seismic rehabilitation of existing buildings. ASCE 41. Reston (VA): American Society of Civil Engineers; 2007.
- [47] Tao Tan. Research on mechanical behavior of high strength bolt-jointed assembled Concrete Wallboard (Master degree Thesis). Changsha: Central South University; 2018. (in Chinese).
- [48] Graziotti F, Tomassetti U, Kallioras S, et al. Shaking table test on a full scale URM cavity wall building. *Bull Earthq Eng* 2017;15(12):5329–64.
- [49] Mendes N, Lourenço PB, Campos-Costa A. Shaking table testing of an existing masonry building: assessment and improvement of the seismic performance. *Earthquake Eng Struct Dyn* 2014;43(2):247–66.
- [50] Cosenza E, Sarno LD, Maddaloni G, et al. Shake table tests for the seismic fragility evaluation of hospital rooms. *Earthquake Eng Struct Dyn* 2015;44(1):23–40.
- [51] Porter K, Kennedy R, Bachman R. Creating fragility functions for performance-based earthquake engineering. *Earthquake Spectra* 2007;23(2):471–89. <https://doi.org/10.1193/1.2720892>.
- [52] FEMA. HAZUS99 Technical Manual. Washington DC: Federal Emergency Management Agency; 1999.